

Bulk Doping of Millimeter-Thick Conjugated Polymer Foams for Plastic Thermoelectrics

Renee Kroon,* Jason D. Ryan, David Kiefer, Liyang Yu, Jonna Hynynen, Eva Olsson, and Christian Müller*

Foaming of plastics allows for extensive tuning of mechanical and physicochemical properties. Utilizing the foam architecture for plastic semiconductors can be used to improve ingress of external molecular species that govern the operation of organic electronic devices. In case of plastic thermoelectrics, utilizing solid semiconductors with realistic (millimeter (mm)-thick) dimensions does not permit sequential doping—while sequential doping offers the higher thermoelectric performance compared to other methods—because this doping methodology is diffusion limited. In this work, a fabrication process for poly(3-hexylthiophene) (P3HT) foams is presented, based on a combination of salt leaching and thermally induced phase separation. The obtained micro- and nanoporous architecture permits rapid and uniform doping of mm-thick foams with 2,3,5,6-tetrafluoro-7,7,8,8-tetracyanoquinodimethane, while thick solid P3HT structures suffer from protracted doping times and a dopant-depleted central region. Importantly, the thermoelectric performance of a P3HT foam is largely retained when normalized with regard to the quantity of used material.

1. Introduction

Foaming of plastics is a widely used strategy to alter their surface area and physicochemical properties, using pore size, connectivity of the pores, and porosity as design tools.^[1] The low weight combined with a high degree of compressibility (low Poisson's ratio) found in foams of common polymers such as polystyrene and polyurethanes makes them particularly suitable for packaging and cushioning. In addition, the already low thermal conductivity of polymers such as polystyrene and polyisocyanurate can be further decreased for various insulating purposes, from food delivery to building construction.^[2,3] The porous nature of foams facilitates ingress of gases and liquids, for example water in poly(vinyl alcohol)

sponges or bodily fluids in biomedical scaffolds.^[4] Recently, poly(3,4-ethylenedioxythiophene):poly(styrene sulfonate)-based formulations were used to fabricate electronic aerogels via lyophilization for applications, such as supercapacitors, pressure sensors, thermoelectrics, and bioelectronics.^[5–10]

Conjugated polymers are widely considered for applications such as bioelectronics and thermoelectrics that require the infiltration of solid samples with external molecular species. However, the diffusion of a molecular species into a solid semiconductor is generally slow. For example, the migration of fullerenes in poly(3-hexylthiophene) (P3HT)^[11,12] or poly[9,9-bis(2-ethylhexyl)fluorene]^[13] occurs with a temperature-dependent diffusion coefficient of not more than 10^{-15} – 10^{-13} m² s⁻¹ above the glass transition temperature.^[14] A similar diffusion

coefficient of 2.5×10^{-15} m² s⁻¹ was found for iodine diffusion in P3HT at room temperature (RT), despite iodine being a smaller molecule than fullerenes.^[15]

To render polymer semiconductors suitable for organic thermoelectrics, the charge carrier density must be optimized through introduction of molecular dopants such as 2,3,5,6-tetrafluoro-7,7,8,8-tetracyanoquinodimethane (F4TCNQ).^[16–19] At the same time, thick, millimeter (mm)-sized doped semiconductor structures are required for optimal thermoelectric performance.^[18,20] While coprocessing of the dopant and semiconductor from the same solution pre-eminently suits the preparation of bulky thermoelectric materials as it is a convenient, one-step process,^[21–24] sequential doping—although a two-step process—offers superior thermoelectric properties.^[23,25–30] This is because the latter allows optimization of the solid-state nanostructure of the organic semiconductor prior to doping.

Unfortunately, sequential doping of thick, solid semiconductor structures is extremely difficult because the introduction of dopant molecules is diffusion limited. Thus far, processing of organic thermoelectric materials has been limited to thin layers of doped semiconductors that are then print laminated^[31] or folded^[32] to create thick architectures. Ultimately, tools that permit to introduce large, slowly diffusing dopant molecules into bulk structures will become essential as it simultaneously results in higher thermal stability of the final material^[33] or mitigates the drift of dopant molecules due to an electric field.^[34]

Dr. R. Kroon, J. D. Ryan, D. Kiefer, Dr. L. Yu, J. Hynynen, Prof. C. Müller
Department of Chemistry and Chemical Engineering
Chalmers University of Technology
41296 Göteborg, Sweden
E-mail: renee.kroon@chalmers.se; christian.muller@chalmers.se

Prof. E. Olsson
Department of Physics
Chalmers University of Technology
41296 Göteborg, Sweden

 The ORCID identification number(s) for the author(s) of this article can be found under <https://doi.org/10.1002/adfm.201704183>.

DOI: 10.1002/adfm.201704183

Here, we establish that semiconductor foams readily permit sequential doping of thick semiconductor structures by assisting the transport of the dopant. We demonstrate that thermally induced phase separation (TIPS) combined with salt leaching can be used to fabricate centimeter (cm)-sized P3HT foams with a porosity of $66\% \pm 4\%$ and a microporous internal structure that is interconnected with nanopores. The dopant uptake of 1.5 mm-thick P3HT foams is probed via immersion doping with F4TCNQ and found to be at least eight times faster than $400 \mu\text{m}$ thick solid P3HT samples that, in addition, exhibit an internal F4TCNQ-depleted region. Finally, the thermoelectric properties of doped P3HT foam and solid P3HT are compared, revealing that the figure of merit is not severely compromised when normalized with regard to the quantity of used material.

2. Results and Discussion

To obtain semiconductor foams, we modified an experimental procedure described by Heijkants et al., who reported the fabrication of porous biocompatible meniscal scaffolds via TIPS + salt leaching approach.^[35,36] The salt porogen is used to introduce micrometer-sized pores of which the size can be controlled by the dimensions of the salt crystals. TIPS results in the formation of a polymer-rich phase and a polymer-lean phase,^[37] creating small-sized pores in the polymer that form continuous pathways to facilitate salt leaching and prevent intercalation of

isolated salt crystals. Several characteristic requirements exist when fabricating foams with this approach. First, a very concentrated, homogeneous polymer solution with (ideally) moderate processing temperatures should be used. Therefore, we chose to use P3HT (88% regioregular, M_w : 56 kg mol^{-1}) combined with 1,2-dichlorobenzene (oDCB) as the diluent because of its high compatibility with the polymer. Second, the homogeneous polymer mixture should exhibit TIPS upon cooling, either via liquid–liquid (L–L)^[38] or liquid–solid (L–S)^[39] phase separation to interconnect the pores that arise from salt leaching. We will then exploit the same network of pores to assist in rapid distribution of the dopant solution throughout P3HT foam structures.

We started by establishing a foam fabrication process that can be performed without excessive cooling or heating. To determine appropriate processing parameters, we first focused on constructing a phase diagram of P3HT:oDCB solutions for relevant compositions and a temperature window of $20 \text{ }^\circ\text{C} < T_{\text{processing}} < 120 \text{ }^\circ\text{C}$ (Figure 1). Differential scanning calorimetry (DSC) cooling traces ($T_{\text{cool}} = 2 \text{ }^\circ\text{C min}^{-1}$) of P3HT:oDCB solutions with varying volume fractions of P3HT (ϕ_{P3HT}) were recorded and the onset of the main exothermal transitions was extracted (Figure S1, Supporting Information). For less concentrated solutions with $\phi_{\text{P3HT}} \leq 0.05$ we observe a single exotherm, indicating that crystallization occurs from a homogeneous solution. Instead, for more concentrated solutions with $\phi_{\text{P3HT}} > 0.05$ two exotherms are present, which suggests that L–L phase separation precedes crystallization of the

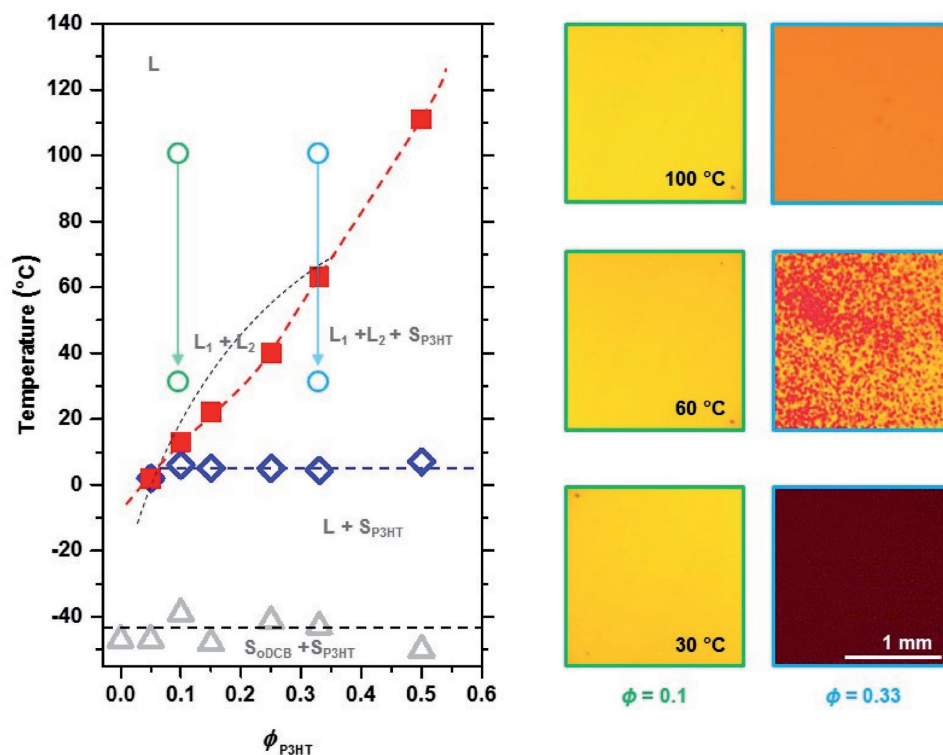


Figure 1. Left, phase diagram based on cooling of P3HT:oDCB solutions with varying compositions ($T_{\text{cool}} = -2 \text{ }^\circ\text{C min}^{-1}$). L: homogeneous mixture; $L_1 + L_2$: liquid–liquid phase separation; $L_1 + L_2 + S_{\text{P3HT}}$: P3HT crystallization in the polymer-rich phase; $L + S_{\text{P3HT}}$: P3HT crystallization in the polymer-lean phase; $S_{\text{oDCB}} + S_{\text{P3HT}}$: crystallization of oDCB. Right, corresponding optical microscopy images of P3HT:oDCB solutions at various temperatures ($t_{\text{isothermal}} = 5 \text{ min}$) for $\phi_{\text{P3HT}} = 0.33$ and $\phi_{\text{P3HT}} = 0.1$.

polymer. P3HT first crystallized from a polymer-rich phase (first exotherm) followed by crystallization from a polymer-lean phase at lower temperatures (second exotherm).

To further investigate if P3HT:oDCB binaries undergo an L-L or L-S phase separation (or both) and for which compositions above room temperature, we used optical microscopy to monitor the microstructure of solutions with $\phi_{\text{P3HT}} = 0.1$ and $\phi_{\text{P3HT}} = 0.33$ during gradual isothermal cooling from 100 °C to 30 °C (Figure S2, Supporting Information). No apparent phase separation was observed during cooling of solutions with $\phi_{\text{P3HT}} = 0.1$ (Figure 1, green arrow) to RT. In contrast, upon cooling of the solution with $\phi_{\text{P3HT}} = 0.33$ (Figure 1, blue arrow), red P3HT-rich domains started to emerge during $T_{\text{isothermal}} = 60$ °C, which gradually turn purple, indicative of P3HT crystallization. We conclude that in case of sufficiently concentrated solutions, L-L phase separation occurs prior to solidification. The latter is similar to the work by Hellmann et al. who studied solidification of P3HT:polyethylene oxide:chloroform ternary blends via controlled solvent evaporation and found that after L-L phase separation the P3HT-rich phase underwent crystallization which manifested itself as a distinct color change from orange-red to purple.^[40]

To illustrate the observed phase separation behavior, we constructed a temperature–composition phase diagram for P3HT:oDCB. At sufficiently elevated temperatures only a homogeneous mixture (L) exists. As the temperature is lowered for $\phi_{\text{P3HT}} > 0.05$, phase separation from $L \rightarrow L_1 + L_2$ occurs. L-L phase separation leads to the formation of a polymer-rich and a polymer-lean phase. Note that we were unable to detect the $L_1 + L_2$ coexistence line below which L-L phase separation occurs (outlined by the dotted line in Figure 4). For $\phi_{\text{P3HT}} > 0.05$ and $T > 5$ °C a region exists where P3HT crystallizes in the polymer-rich phase ($L_1 + L_2 + S_{\text{P3HT}}$). For $T < 5$ °C, solid P3HT is also present for lower concentrations ($L + S_{\text{P3HT}}$) and for $T < -40$ °C the solvent crystallizes ($S_{\text{oDCB}} + S_{\text{P3HT}}$).

For foam formation, we choose to employ a solution with $\phi_{\text{P3HT}} = 0.33$, as this concentration offers a homogeneous solution with high P3HT content at moderately high temperatures while exhibiting TIPS well above room temperature. P3HT foams were fabricated according to the scheme depicted in **Figure 2**. First, P3HT and oDCB were mixed in a 33% v/v ratio at 100 °C until a homogeneous, red viscous mixture was obtained. Small NaCl crystals (≤ 20 μm) were used as such dimensions would result in a more uniform foam structure and were obtained via previously reported precipitation method.^[41] The amount of NaCl was chosen to yield a foam with a theoretical porosity of $\approx 80\%$. The NaCl porogen was subsequently mixed with the P3HT:oDCB mixture until a homogeneous paste

was obtained, then cooled slowly to allow for TIPS to occur. Finally, the mixture was left to cool at ambient overnight to ensure that the same temperature was reached throughout the sample. Then, the solidified mixture was immersed in methanol (MeOH) as this acts as an orthogonal solvent for P3HT. While oDCB could be leached out with pure MeOH (≈ 72 h.), virtually complete removal of NaCl required addition of water to the MeOH phase (10–50%) and ≈ 3 weeks of leaching for 1 cm-thick foams. We like to note that thinner samples (≈ 1 mm thickness) could be salt leached within 1 d. During salt leaching, the foams appeared to decrease about 10% in volume, which we explain by the contraction of the P3HT phase after removal of the oDCB diluent. Nevertheless, P3HT foams with a diameter ≈ 25 mm, height ≈ 10 mm, and a porosity of $66\% \pm 4\%$ were obtained (Figure S3, Supporting Information, average of 19 samples). After drying of the P3HT foam, elemental analysis was performed to confirm that only minute amounts of NaCl were still present; 0.1% m/m at the edge and 1% m/m at the center of the foam, which shows that the removal of NaCl from a 10 mm thick specimen was close to complete. Scanning electron microscopy (SEM) was subsequently used to investigate the P3HT foams, revealing a microporous structure that arises from the NaCl porogen leaching (**Figure 3**), with P3HT wall thickness on the order of 1 μm . These micropores (size 14 ± 6 μm) are interconnected by nanometer-sized pores (diameter $\approx 63 \pm 19$ nm) that most likely stem from the crystallization that occurs in the P3HT-rich phase.

To investigate if manipulation of the P3HT solid-state structure was possible without collapse of the delicate internal pore structure, we performed an annealing experiment. A foam sample was annealed for 30 min at 150 °C and subsequently analyzed by wide-angle X-ray scattering (WAXS) and SEM (Figure 3). SEM images indicate that the open microporous structure of the P3HT foam is retained, evidence by the unchanged size of the macropores (size 14 ± 6 μm). The nanopores in the P3HT phase also persist but their density and size (diameter $\approx 54 \pm 19$ nm) has decreased slightly, as the annealing step introduces some mobility in the P3HT phase. WAXS indicates a more ordered solid-state structure of P3HT as evidenced by the larger area ($\approx 11\%$) of the 100 lamellar stacking peak and the increased correlation length, $L_{\text{corr}} \approx 12.4$ nm and $L_{\text{corr}} \approx 15.2$ nm for pristine and annealed foam, respectively. Thus, we conclude that manipulation of the P3HT nanostructure could be carried out without significant changes in the foam architecture.

In a next set of experiments, we studied the uptake of dopant by P3HT. We chose to work with F4TCNQ as the dopant, as P3HT:F4TCNQ represents a well-studied

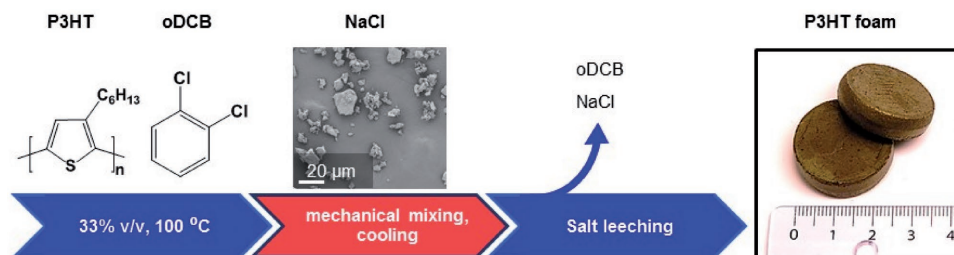


Figure 2. Flow chart of salt-leaching method for P3HT foam fabrication.

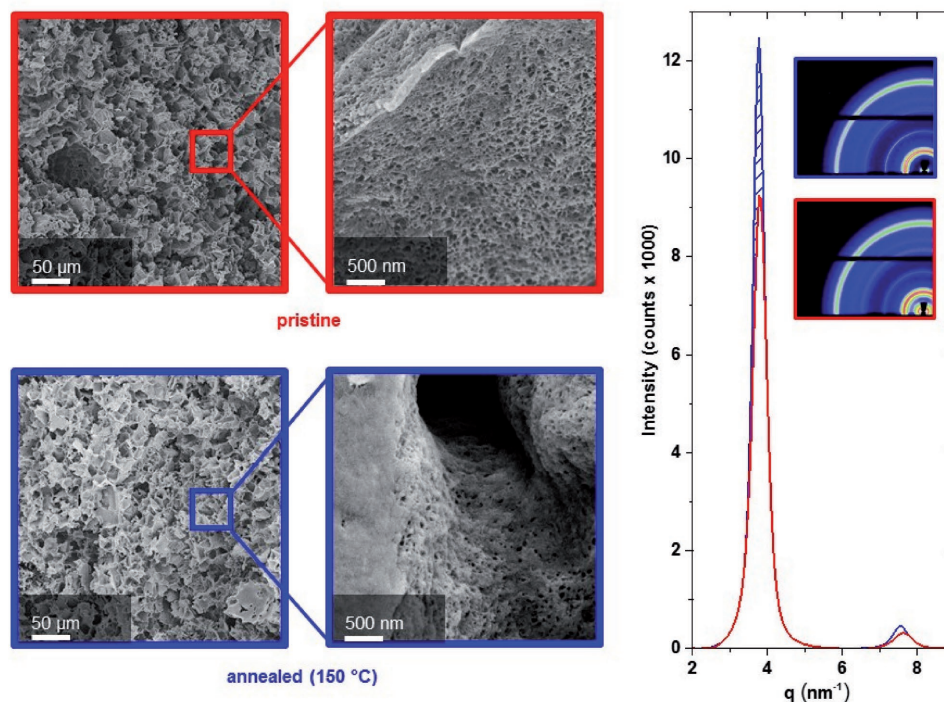


Figure 3. Left: SEM microscopy images of the P3HT foam before (red, top) and after annealing for 30 min at 150 °C (blue, bottom). Right, lamellar stacking peak in the WAXS spectra and 2D plot (inset) of pristine (red) and annealed (blue) foams.

semiconductor/dopant combination.^[19,21–24,26,27,29,42] We compared the dopant uptake of 1.5 mm thick P3HT foams with 400 μm thick solid P3HT samples. To confirm that the difference in dopant uptake does not arise due to a different nanostructure of P3HT we carried out DSC (Figure S4, Supporting Information). The melting exotherms are similar in shape with a prominent melting peak at 235 °C and 237 °C for solid and foam samples, respectively. This indicates a comparable lamellar thickness for the majority of the crystals in each material. For the degree of crystallinity of each material we find ≈44% and ≈35% for solid film and foam, respectively, using $\Delta H_u = 49 \text{ J g}^{-1}$ as the enthalpy of fusion.^[43]

Samples were doped with 20 mol% F4TCNQ which was calculated relative to the molar concentration of available P3HT monomeric units. Note that we employed a low dopant mass concentration of $\rho_{\text{F4TCNQ}} \approx 1 \text{ g L}^{-1}$ F4TCNQ in 1:1 acetonitrile (ACN):dichloromethane (DCM) to allow for accurate stoichiometry between the polymer and dopant. We determined the dopant uptake by gravimetric analysis, which allowed us to record the sample weight before and after immersion in the dopant solution while varying the doping time.

The foam structure permits rapid uptake of the dopant, incorporating the vast majority of F4TCNQ into the P3HT foam after 4 h of immersion doping, and enters a saturated regime after 10 h. In contrast, even after 3 d of immersion doping, saturation of the F4TCNQ uptake has not yet been reached for the solid samples, despite being half the weight of the foam samples. To further illustrate the difference in dopant uptake, we estimated the initial rate of F4TCNQ uptake for each sample, 0.01 mol% h⁻¹ and 0.4 mol% h⁻¹ for solid and foam samples, respectively. To probe if the foam doping process could be

further accelerated, we used a more concentrated F4TCNQ solution ($\rho_{\text{F4TCNQ}} \approx 10 \text{ g L}^{-1}$). Doping was further assisted by quickly exchanging the air with dopant solution by applying vacuum for ≈1 s. In this way, the foam could be completely doped after 1 h of immersion doping, corresponding to an F4TCNQ uptake of 8 mol% h⁻¹.

To investigate the ingress of F4TCNQ in the P3HT samples, we performed energy-filtered dispersive X-ray spectroscopy (EDX) on cross-sections of each sample type to qualitatively probe the fluorine, carbon, and sulfur signals (Figure 4, bottom and Figure S5, Supporting Information). The foam sample shows a comparable intensity of the fluorine signal throughout its interior structure, indicating that the F4TCNQ is distributed evenly inside the P3HT foam. In sharp contrast, after 72 h doping the F4TCNQ appears to accumulate at the edge with a F4TCNQ-depleted region in the center of each solid sample. Thus, despite having incorporated the majority of F4TCNQ, the dopant is unable to completely diffuse to the center of the sample, leading to a prominent gradient. The dopant uptake studies show that sequential doping of large solid architectures indeed proves to be difficult and that thick P3HT foams can be doped much more rapidly and more uniformly compared to solid samples.

To establish if, and to what extent the thermoelectric performance of foams is affected relative to solid structures, we compared the thermoelectric parameters of P3HT foams with solid P3HT samples after sequential doping with F4TCNQ. We expect a decrease in electrical conductivity of the foams due to the large air content and the increased tortuosity of conducting pathways.^[44] Regarding the Seebeck coefficient, effective medium theories imply that the Seebeck of a doped

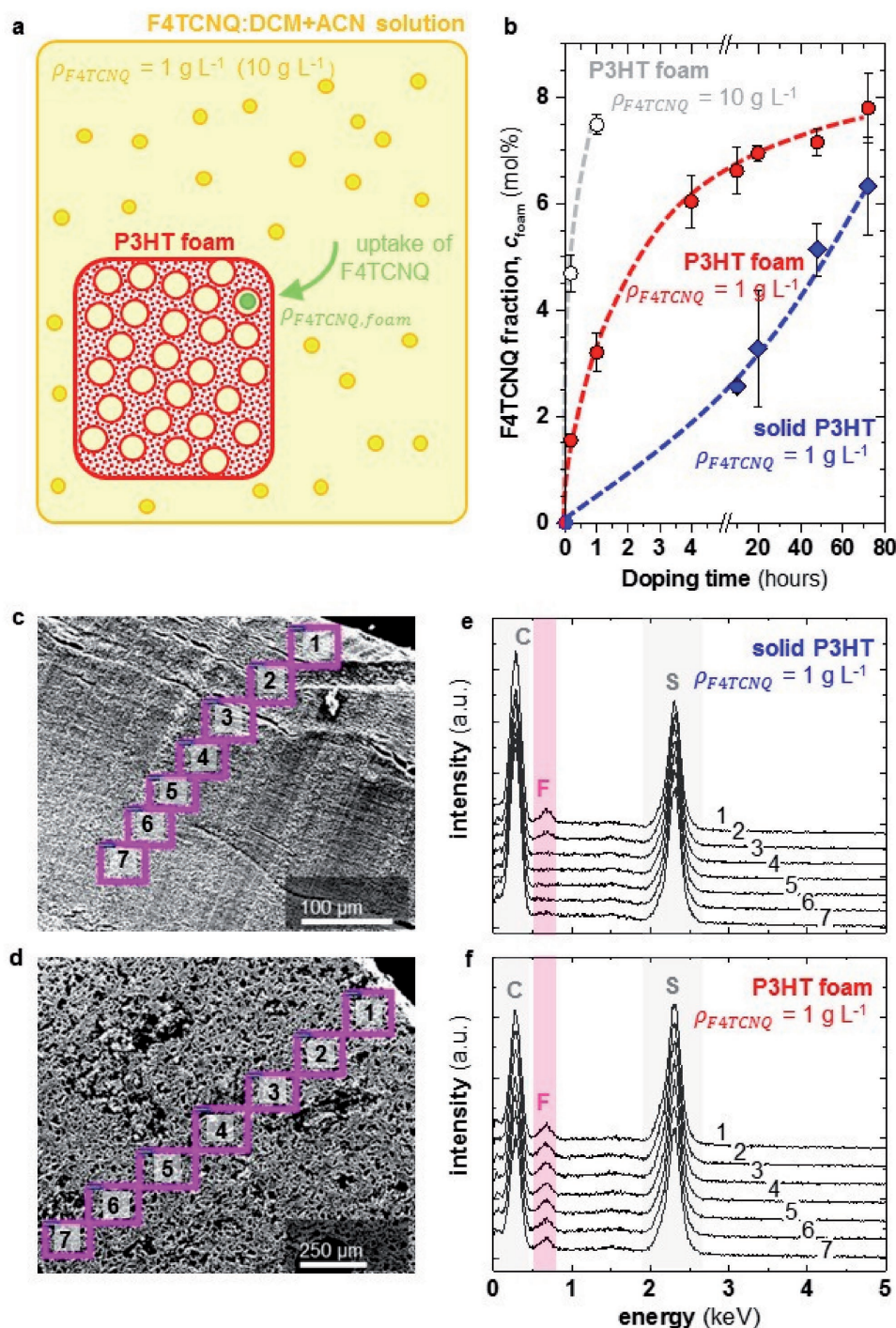


Figure 4. a) Schematic overview of the conducted dopant uptake experiment. b) Uptake of F4TCNQ in mol% as function of doping time for foam (red circles) and solid samples (blue diamonds) for low concentration of the dopant solution, and for foams doped with high concentration of the dopant solution (white circles). Dashed lines are a guide to the eye. Sample dimensions: $l \times w \times h$, weight are $\approx 10 \text{ mm} \times 1.5 \text{ mm} \times 1.5 \text{ mm}$, 10 mg for foams and $\approx 10 \text{ mm} \times 1.5 \text{ mm} \times 0.4 \text{ mm}$, and 5 mg for films. c–f) Probed areas for carbon (C), sulfur (S), and fluorine (F) and the corresponding EDX spectra for each area of c,e) solid P3HT and d,f) P3HT foam after 72 h immersion doping with F4TCNQ.

P3HT foam is the sum of the Seebeck of air and doped P3HT, weighted by the relative electrical conductivity. Since the electrical conductivity of air is extremely small (on the order of 10^{-14} – $10^{-15} \text{ S cm}^{-1}$), the contribution of air to the Seebeck coefficient of a foam will also be extremely small. Thus, foaming

a material does not alter its Seebeck coefficient (for the same electrical conductivity of each solid material). For the measurement of the electrical conductivity and Seebeck coefficient, we used two sets of foam samples that were doped with different sequential doping methodologies. One set of foam samples was

doped stepwise, to control the doping level with the number of doping cycles, via deficit amount of F4TCNQ in the dopant solution. For the electrical conductivity, we immersion doped five foam samples repeatedly with 4 mol% of F4TCNQ (1:1 ACN:DCM, $\rho_{\text{F4TCNQ}} \approx 1 \text{ g L}^{-1}$) according to weight and measured the electrical conductivity of the sample after each doping step (20 h). Corresponding samples for the Seebeck measurements were doped in the same stepwise manner but each data point consumed a set of three foams. We chose this procedure because our Seebeck measurement setup requires fixation of each sample to the sample stage, which prevents recycling of the foam samples. More details of the sample preparation can be found in the Supporting Information. For the second set of samples, foam samples from the dopant uptake study were used, as the dopant concentration in the sample varies with doping time (10 min–4 h) and the concentration of the dopant solution ($\rho_{\text{F4TCNQ}} \approx 1\text{--}10 \text{ g L}^{-1}$). To obtain reliable values for the electrical conductivity and Seebeck coefficient of solid samples we used much thinner 5 μm thick P3HT films, as the 400 μm thick samples proved difficult to dope but also bent and cracked during immersion doping (Figure S6, Supporting Information). P3HT films (three per data set) were immersion doped for 24 h using a range of dopant solution concentrations ($\rho_{\text{F4TCNQ}} \approx 5 \times 10^{-3}$ to 1 g L^{-1}) to obtain various degrees of doping.

The electrical conductivity and Seebeck coefficient of doped P3HT foams, and solid P3HT samples were subsequently measured (Figure 5, also Figure S16, Supporting Information for electrical conductivity and Seebeck coefficient as function of the used doping conditions). For both solid samples and foams, the Seebeck coefficient α and the electrical conductivity σ follow the empirical relationship $\alpha \propto \sigma^{-1/4}$ that was proposed by Glaudell et al.^[22] However, the trend observed for solid samples is shifted in accordance with their higher

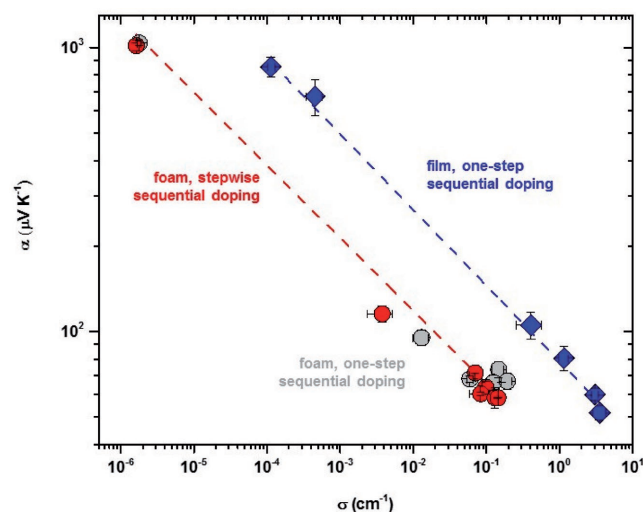


Figure 5. Logarithmic plot of Seebeck coefficient α as function of electrical conductivity σ of P3HT foams and films after immersion doping with F4TCNQ: foam samples ($l \times w \times h \approx 10 \text{ mm} \times 1.5 \text{ mm} \times 1.5 \text{ mm}$) stepwise sequentially doped with 4% F4TCNQ for 20 h per doping step (red circles) or in one step (gray circles) with varying dopant concentration ($\rho_{\text{F4TCNQ}} = 1$ or 10 g L^{-1}) and doping times ($t_{\text{doping}} = 10 \text{ min}, 1 \text{ h}$ or 4 h); solid 5 μm thick dropcast P3HT films sequentially doped for 24 h ($\rho_{\text{F4TCNQ}} = 0.005, 0.01, 0.05, 0.1, 0.5, \text{ and } 1 \text{ g L}^{-1}$).

electrical conductivity, and we find a maximum average $\sigma_{\text{solid}} = 3.5 \pm 0.7 \text{ S cm}^{-1}$ combined with $\alpha_{\text{solid}} = 52 \pm 3 \mu\text{V K}^{-1}$. For the stepwise sequentially doped foams, a maximum average value of $\sigma_{\text{foam}} = 0.14 \pm 0.03 \text{ S cm}^{-1}$ was obtained, paired with a minimum value of $\alpha_{\text{foam}} = 58 \pm 1 \mu\text{V K}^{-1}$. For samples that were doped in one step with higher dopant concentration and shorter doping times, we find a similar maximum average value of $\sigma_{\text{foam}} = 0.19 \pm 0.03 \text{ S cm}^{-1}$ but a slightly higher corresponding value of $\alpha_{\text{foam}} = 67 \pm 5 \mu\text{V K}^{-1}$. Gratifyingly, foam samples that were doped with either $\rho_{\text{F4TCNQ}} \approx 1 \text{ g L}^{-1}$ for 4 h or $\rho_{\text{F4TCNQ}} \approx 10 \text{ g L}^{-1}$ for 1 h display similar electrical conductivities, which is in agreement with the similar amount of dopant that was taken up by each sample (cf. Figure 4).

The evolution of the electrical conductivity with the porosity of a material can be approached by various models that describe the evolution of the relative electrical conductivity (σ_r) with volume fraction porosity (V_p) for open- or close-cell foams. To evaluate the experimentally obtained electrical conductivity of our P3HT foam compared to solid-doped P3HT, we use the differential effective medium approach to estimate the relative electrical conductivity^[45,46]

$$\sigma_r = (1 - V_p)^n \quad (1)$$

with n being a shape factor ($n = 1.5$ for spheres) based on the change in conductivity of a matrix containing randomly located overlapping spheres. We chose to use this closed-cell model because it has shown to provide good agreement with experimental data, and we define our foams as closed-cell because of the presence of cells walls (even though the walls are porous). Theoretically, for $V_p = 0.66$ and $n = 1.5$, we find a relative electrical conductivity of $\sigma_r = 0.19$, or a factor of 5 difference between solid and foam samples. Experimentally, the loss in the electrical conductivity of the foam is a factor of 9 which likely is due to an underestimation of the tortuosity in the solid phase, due to the cubic cell shape, the presence of nanopores in the solid, or discontinuities in the foam structure such as dead ends or cell walls that are oriented perpendicular to the applied electrical field.

We went on to measure the thermal conductivity of solid and foam samples. We carried out thermal conductivity measurements on millimeter-thick samples using a Hotdisk setup, where a thin-film heating coil is placed between two identical slabs of material (see Experimental Section for details). Both, the in-plane and out-of-plane thermal conductivity, κ_{\parallel} and κ_{\perp} , can be determined with this method. For the here investigated samples we observe no anisotropy and therefore we focus our analysis on the average thermal conductivity (see the Supporting Information). To determine the thermal conductivity of solid P3HT, we fabricated samples by pressing powder of neat P3HT as well as P3HT doped with 8 mol% F4TCNQ into pellets at room temperature, followed by pressing at 80 and 150 $^{\circ}\text{C}$, respectively, to ensure a homogeneous internal structure and probe surface. For solid samples of neat and doped P3HT we find a similar thermal conductivity of 0.34 ± 0.01 and $0.32 \pm 0.01 \text{ W m}^{-1} \text{ K}^{-1}$, respectively, which is in agreement with previously reported values (0.33 and $0.26 \text{ W m}^{-1} \text{ K}^{-1}$).^[24] We rationalize the similar thermal conductivity of neat and doped P3HT with the relatively low electrical conductivity of these

Table 1. Thermoelectric parameters obtained for doped foam and solid samples doped in one step.

	p [%]	σ [S cm ⁻¹]	α [μ V K ⁻¹]	κ [W m ⁻¹ K ⁻¹]	ZT	ZT'	ZT_{\max}
Solid	0	1.8 ^{a)}	67	0.32 ± 0.01	8 × 10 ⁻⁴	8 × 10 ⁻⁴	
Solid max		3.24	58.1				1.0 × 10 ⁻³
Foam	66	0.19 ± 0.03	67	0.14 ± 0.01	2 × 10 ⁻⁴	6 × 10 ⁻⁴	
Foam max		0.22	68.4				2.3 × 10 ⁻⁴

^{a)}Extrapolated value for a Seebeck coefficient of 67 μ V K⁻¹ using the trend line for solid samples in Figure 5.

samples. Assuming that the Wiedemann–Franz law holds,^[47] we estimate that the electronic contribution to the thermal conductivity is on the order of 10⁻³ W m⁻¹ K⁻¹), which is within the estimated error of our measurements.

We expect a decrease in thermal conductivity for the foams, as they consist to $p = 66\%$ of air, which has a very low thermal conductivity. Since the pores of our P3HT foams are much larger than the mean free path of air, we can use the rule of mixtures to estimate the thermal conductivity of the foam

$$\kappa_{\text{foam}} = \kappa_{\text{P3HT}} \left(1 - \frac{p}{100}\right) + \kappa_{\text{air}} \frac{p}{100} \quad (2)$$

where κ_{P3HT} and $\kappa_{\text{air}} = 0.025$ W m⁻¹ K⁻¹ are the thermal conductivity of solid P3HT and air, respectively, and p is the porosity of the foam in percent.^[48] We estimate a value of $\kappa_{\text{foam}} = 0.12$ W m⁻¹ K⁻¹ for a foam with a porosity of 66%, using for κ_{P3HT} the value measured for solid P3HT, $\kappa_{\text{P3HT}} \approx 0.3$ W m⁻¹ K⁻¹. For both 4 mm thick samples of neat foam and foam doped with 8 mol% F4TCNQ we measure the same thermal conductivity of $\kappa_{\text{foam}} = 0.14 \pm 0.01$ W m⁻¹ K⁻¹, which is in good agreement with the theoretically predicted value.

To compare the thermoelectric performance of doped solid samples and P3HT foams, we calculated the figure of merit

$$ZT = \frac{\alpha^2 \sigma}{\kappa} T \quad (3)$$

where T is the absolute temperature, which we set to 300 K. For doped foams we find a value of $ZT \approx 2 \times 10^{-4}$ (Table 1). We use the trend line for $\alpha(\sigma)$ of solid samples in Figure 5 to extrapolate a value for σ that corresponds to the same Seebeck coefficient $\alpha = 66.8$ μ V K⁻¹ that was used to calculate the ZT of the doped foam. For the same Seebeck coefficient, we find a four times higher value of $ZT \approx 8 \times 10^{-4}$ for solid P3HT samples. Comparing the maximum figure of merit for each material, calculated by using the highest achieved thermoelectric parameters, we find the same ratio between the figure of merit, $ZT_{\max} \approx 2.3 \times 10^{-4}$ and $ZT_{\max} \approx 1 \times 10^{-3}$ for foam or solid samples, respectively.

The lower ZT of the foams is due to the decrease in electrical conductivity, which is not compensated for by the lower thermal conductivity of the foam. We chose to compare our results with regard to the amount of material that is used to prepare the thermoelectric material. The comparison is made under the conditions that the increase in foam sample size is accommodated

only by the area while keeping the thickness constant (effectively increasing the conductance of the foam sample).

We use the following modified figure of merit that is normalized by the porosity of the sample

$$ZT' = \frac{\alpha^2 \sigma}{\kappa} T \times \frac{100}{100 - p} \quad (4)$$

Comparison of this normalized figure of merit indicates that P3HT foams give rise to a similar $ZT' \approx 6$ and 8×10^{-4} for foams and solid samples, respectively. We conclude that the thermoelectric performance of a given amount of material is not severely compromised when using foam structures, which allows to exploit other advantages such as here demonstrated ability to dope bulk samples more rapidly. Further, we like to point out that methods, which permit to alter the thermal conductivity of a material, can be used to optimize the dimensions of a thermoelectric generator.^[49,50] Therefore, we argue that foaming of organic semiconductors represents a powerful tool for the design of plastic thermoelectric materials.

3. Conclusion

To summarize, we have demonstrated that TIPS combined with salt leaching is a promising route to produce semiconductor foams. The foam architecture allows doping of mm-thick semiconductor structures much faster and more uniformly compared to solid semiconductors. Thus, for the first time we were able to use sequential doping, which is known to result in improved thermoelectric performance, in combination with thick samples. As the thermoelectric performance of the P3HT foam is almost retained per quantity of material, thermoelectric foams could be particularly promising for large area applications where device area is not a limiting factor, e.g., cladding of chimneys and factory pipes with plastic thermoelectric generators. Foaming of plastic semiconductors, in particular the fabrication of thin porous films via TIPS, represents an interesting avenue to explore, to, for example, improve ingress of external molecular species, or to increase surface area in organic sensors and electronic membranes.

Supporting Information

Supporting Information is available from the Wiley Online Library or from the author.

Acknowledgements

Financial support from the Swedish Research Council Formas, the Knut and Alice Wallenberg Foundation through a Wallenberg Academy Fellowship, and the European Research Council (ERC) under Grant No. 637624 is gratefully acknowledged. The authors thank the Cornell High Energy Synchrotron Source (CHESS) (supported by the NSF & NIH/NIGMS via NSF award DMR-1332208) for providing experimental time for WAXS measurements.

Conflict of Interest

The authors declare no conflict of interest.

Keywords

bulk doping, conjugated polymer foam, plastic thermoelectrics, poly(3-hexylthiophene), thermal conductivity

Received: July 25, 2017

Revised: August 31, 2017

Published online: October 24, 2017

- [1] A. Cunningham, N. C. Hilyard, in *Low Density Cellular Plastics: Physical Basis of Behaviour* (Eds.: N. C. Hilyard, A. Cunningham), Springer, Dordrecht, The Netherlands **1994**, p. 1.
- [2] J. Gagliani, D. E. Supkis, *Acta Astronaut.* **1980**, *7*, 653.
- [3] C. Forest, P. Chaumont, P. Cassagnau, B. Swoboda, P. Sonntag, *Prog. Polym. Sci.* **2015**, *41*, 122.
- [4] P. Netti, *Biomedical Foams for Tissue Engineering Applications*, (Ed.: P. Netti), Woodhead Publishing, Sawston, Cambridge **2014**, xv.
- [5] M. P. Gordon, E. W. Zaia, P. Zhou, B. Russ, N. E. Coates, A. Sahu, J. J. Urban, *J. Appl. Polym. Sci.* **2016**, *134*, 44070.
- [6] Z. U. Khan, J. Edberg, M. M. Hamed, R. Gabrielsson, H. Granberg, L. Wägberg, I. Engquist, M. Berggren, X. Crispin, *Adv. Energy Mater.* **2016**, *28*, 4556.
- [7] X. Yang, K. Shi, I. Zhitomirsky, E. D. Cranston, *Adv. Energy Mater.* **2015**, *27*, 6104.
- [8] F. Zhang, Y. Zang, D. Huang, C.-A. Di, D. Zhu, *Nat. Commun.* **2015**, *6*, 6269.
- [9] A. M.-D. Wan, S. Inal, T. Williams, K. Wang, P. Leleux, L. Estevez, E. P. Giannelis, C. Fischbach, G. G. Malliaras, D. Gourdon, *J. Mater. Chem. B* **2015**, *3*, 5040.
- [10] S. Inal, A. Hama, M. Ferro, C. Pitsalidis, J. Ozat, D. Iandolo, A.-M. Pappa, M. Hadida, M. Huerta, D. Marchat, P. Mailley, R. M. Owens, *Adv. Biosyst.* **2017**, *1*, 1700052.
- [11] N. D. Treat, T. E. Mates, C. J. Hawker, E. J. Kramer, M. L. Chabiny, *Macromolecules* **2013**, *46*, 1002.
- [12] B. Watts, W. J. Belcher, L. Thomsen, H. Ade, P. C. Dastoor, *Macromolecules* **2009**, *42*, 8392.
- [13] F. Fischer, T. Hahn, H. Bässler, I. Bauer, P. Strohriegel, A. Köhler, *Adv. Funct. Mater.* **2014**, *24*, 6172.
- [14] C. Müller, *Chem. Mater.* **2015**, *27*, 2740.
- [15] A. J. Maliakal, *ACS Appl. Mater. Interfaces* **2013**, *5*, 8300.
- [16] O. Bubnova, X. Crispin, *Energy Environ. Sci.* **2012**, *5*, 9345.
- [17] R. Kroon, D. A. Mengistie, D. Kiefer, J. Hynynen, J. D. Ryan, L. Yu, C. Muller, *Chem. Soc. Rev.* **2016**, *45*, 6147.
- [18] B. Russ, A. Gludell, J. J. Urban, M. L. Chabiny, R. A. Segalman, *Nat. Rev. Mater.* **2016**, *1*, 16050.
- [19] I. Salzmann, G. Heimel, M. Oehzelt, S. Winkler, N. Koch, *Acc. Chem. Res.* **2016**, *49*, 370.
- [20] J.-H. Bahk, H. Fang, K. Yazawa, A. Shakouri, *J. Mater. Chem. C* **2015**, *3*, 10362.
- [21] D. T. Duong, C. Wang, E. Antono, M. F. Toney, A. Salleo, *Org. Electron.* **2013**, *14*, 1330.
- [22] A. M. Gludell, J. E. Cochran, S. N. Patel, M. L. Chabiny, *Adv. Energy Mater.* **2015**, *5*, 1401072.
- [23] I. E. Jacobs, E. W. Aasen, J. L. Oliveira, T. N. Fonseca, J. D. Roehling, J. Li, G. Zhang, M. P. Augustine, M. Mascal, A. J. Moule, *J. Mater. Chem. C* **2016**, *4*, 3454.
- [24] D. Kiefer, L. Yu, E. Fransson, A. Gómez, D. Primetzhofer, A. Amassian, M. Campoy-Quiles, C. Müller, *Adv. Sci.* **2016**, 1600203.
- [25] K. Kang, S. Watanabe, K. Broch, A. Sepe, A. Brown, I. Nasrallah, M. Nikolka, Z. Fei, M. Heeney, D. Matsumoto, K. Marumoto, H. Tanaka, S.-I. Kuroda, H. Siringhaus, *Nat. Mater.* **2016**, *15*, 896.
- [26] S. N. Patel, A. M. Gludell, D. Kiefer, M. L. Chabiny, *ACS Macro Lett.* **2016**, *5*, 268.
- [27] D. T. Scholes, S. A. Hawks, P. Y. Yee, H. Wu, J. R. Lindemuth, S. H. Tolbert, B. J. Schwartz, *J. Phys. Chem. Lett.* **2015**, *6*, 4786.
- [28] Q. Zhang, Y. Sun, W. Xu, D. Zhu, *Macromolecules* **2014**, *47*, 609.
- [29] A. Hamidi-Sakr, L. Biniek, J.-L. Bantignies, D. Maurin, L. Herrmann, N. Leclerc, P. Lévêque, V. Vijayakumar, N. Zimmermann, M. Brinkmann, *Adv. Funct. Mater.* **2017**, *27*, 1700173.
- [30] S. N. Patel, A. M. Gludell, K. A. Peterson, E. M. Thomas, K. A. O'Hara, E. Lim, M. L. Chabiny, *Sci. Adv.* **2017**, *3*, e1700434.
- [31] C. A. Hewitt, A. B. Kaiser, S. Roth, M. Craps, R. Czerw, D. L. Carroll, *Nano Lett.* **2012**, *12*, 1307.
- [32] Q. Wei, M. Mukaida, K. Kirihara, Y. Naitoh, T. Ishida, *RSC Adv.* **2014**, *4*, 28802.
- [33] J. Li, C. W. Rochester, I. E. Jacobs, S. Friedrich, P. Stroeve, M. Riede, A. J. Moulé, *ACS Appl. Mater. Interfaces* **2015**, *7*, 28420.
- [34] L. Müller, S.-Y. Rhim, V. Sivanesan, D. Wang, S. Hietzschold, P. Reiser, E. Mankel, S. Beck, S. Barlow, S. R. Marder, A. Pucci, W. Kowalsky, R. Lovrincic, *Adv. Energy Mater.* **2015**, *29*, 1701466.
- [35] R. G. J. C. Heijkants, R. V. Van Calck, J. H. De Groot, A. J. Pennings, A. J. Schouten, *J. Polym. Sci., Part B: Polym. Phys.* **2005**, *43*, 716.
- [36] R. G. J. C. Heijkants, R. V. van Calck, T. G. van Tienen, J. H. de Groot, A. J. Pennings, P. Buma, R. P. H. Veth, A. J. Schouten, *J. Biomed. Mater. Res., Part A* **2008**, *87A*, 921.
- [37] H. E. H. Meijer, *Materials Science and Technology*, Wiley-VCH Verlag GmbH & Co. KGaA, Weinheim **2006**.
- [38] D. R. Lloyd, S. S. Kim, K. E. Kinzer, *J. Membr. Sci.* **1991**, *64*, 1.
- [39] D. R. Lloyd, K. E. Kinzer, H. S. Tseng, *J. Membr. Sci.* **1990**, *52*, 239.
- [40] C. Hellmann, N. D. Treat, A. D. Scaccabarozzi, J. Razzell Hollis, F. D. Fleischli, J. H. Bannock, J. de Mello, J. J. Michels, J.-S. Kim, N. Stingelin, *J. Polym. Sci., Part B: Polym. Phys.* **2015**, *53*, 304.
- [41] F.-H. Marshall, *Phys. Rev.* **1940**, *58*, 642.
- [42] J. Gao, J. D. Roehling, Y. Li, H. Guo, A. J. Moule, J. K. Grey, *J. Mater. Chem. C* **2013**, *1*, 5638.
- [43] C. R. Snyder, R. C. Nieuwendaal, D. M. DeLongchamp, C. K. Luscombe, P. Sista, S. D. Boyd, *Macromolecules* **2014**, *47*, 3942.
- [44] F. G. Cuevas, J. M. Montes, J. Cintas, P. Urban, *J. Porous Mater.* **2008**, *16*, 675.
- [45] A. Kim, M. A. Hasan, S. H. Nahm, S. S. Cho, *Compos. Struct.* **2005**, *71*, 191.
- [46] R. Goodall, L. Weber, A. Mortensen, *J. Appl. Phys.* **2006**, *100*, 044912.
- [47] X. Wang, V. Ho, R. A. Segalman, D. G. Cahill, *Macromolecules* **2013**, *46*, 4937.
- [48] D. S. Smith, A. Alzina, J. Bourret, B. Nait-Ali, F. Pennec, N. Tessier-Doyen, K. Otsu, H. Matsubara, P. Elser, U. T. Gonzenbach, *J. Mater. Res.* **2013**, *28*, 2260.
- [49] W. Glatz, S. Muntwyler, C. Hierold, *Sen. Actuators, A* **2006**, *132*, 337.
- [50] V. Leonov, R. J. M. Vullers, *J. Electron. Mater.* **2009**, *38*, 1491.